A MULTI-RESOLUTION APPROACH TO NON-RIGID REGISTRATION OF MICROSCOPY IMAGES

Kevin S. Lorenz[⋆] *Paul Salama*[†] *Kenneth W. Dunn*[‡] *Edward J. Delp*[⋆]

[⋆]Video and Image Processing Laboratory
School of Electrical and
Computer Engineering
Purdue University
West Lafayette, Indiana

[†]Department of Electrical and
Computer Engineering
Indiana University-Purdue University
Indianapolis, Indiana

[‡]Division of Nephrology
School of Medicine
Indiana University
Indianapolis, Indiana

ABSTRACT

Images collected by intravital microscopy suffer from motion artifacts which necessitates the use of image registration techniques to reconstruct three-dimensional or time series data. In this paper, we describe a multi-resolution/multi-level approach to non-rigid image registration using B-splines with a coarse-to-fine strategy. A control lattice with a coarse grid spacing is used first to account for slowly changing deformations. Next, a control lattice with a finer grid spacing is used to account for more localized and quickly changing deformations. We demonstrate this method on a sequence of images acquired from the lung of a living rat.

Index Terms— image registration, intravital microscopy

1. INTRODUCTION

One of the most exciting forms of microscopy is "intravital microscopy," the technique of microscopic imaging of living animals. Increasingly, intravital multiphoton microscopy is used to collect not just single images, but a series of images, both in time-series and in three-dimensions. Collection of a series of images is complicated by motion resulting from respiration and heartbeat. We describe an image processing method that effectively corrects for motion artifacts in sequences of intravital microscopy images, using an enhanced, multi-resolution non-rigid registration technique using B-splines. This image registration method will aid in segmentation and other image analysis techniques.

2. PROPOSED REGISTRATION METHOD

The non-rigid registration technique described here uses B-splines and is based on the work proposed in [1]. We will extend this technique to use multiple stages in a multi-resolution fashion to further enhance image registration performance. While typically used with only a single pair of grayscale images, we also extend this method to be used with a large series of multi-channel images.

This non-rigid registration method deforms an image by first establishing an underlying mesh of control points. The control points are then optimized such that they maintain a smooth and continuous transformation. A grid of control points, $\phi_{i,j}$, is initially constructed with equal spacings δ_x and δ_y between points, in the horizontal and vertical directions, respectively. The non-rigid transformation $\mathbf{T}$ of a point (x, y) in the image being registered to the corresponding point (x', y') in the reference image is given by the mapping $\mathbf{T}(x, y) \rightarrow (x', y')$ [2]:

$$\mathbf{T}(x,y) = \sum_{l=0}^{3}\sum_{m=0}^{3} B_l(u)B_m(v)\phi_{i+l,j+m} \tag{1}$$

where $i = \lfloor x/\delta_x \rfloor - 1$ and $j = \lfloor y/\delta_y \rfloor - 1$ are the indices of the nearest control point $\phi_{i,j}$ above and to the left of (x, y), and $u = x/\delta_x - \lfloor x/\delta_x \rfloor$ and $v = y/\delta_y - \lfloor y/\delta_y \rfloor$ are such that (u, v) is the relative position of (x, y) relative to $\phi_{i,j}$. Additionally, B_l represents the l-th basis function of the B-spline [3, 4]:

$$\begin{aligned} B_0(t) &= (1-t)^3/6 \\ B_1(t) &= (3t^3 - 6t^2 + 4)/6 \\ B_2(t) &= (-3t^3 + 3t^2 + 3t + 1)/6 \\ B_3(t) &= t^3/6 \end{aligned} \tag{2}$$

The optimal deformation of the grid of control points is found by optimizing a cost function. This cost function includes two terms with two competing goals. The first goal is to maximize the similarity and alignment between the reference image and the image being deformed. The second goal is to smooth and regularize the deformation to create a realistic transformation. The similarity metric, C_{sim}, may be defined as one of numerous possibilities, including sum of squared differences, sum of absolute differences, or normalized mutual information. In this paper, we use sum of log of absolute differences:

$$C_{sim}(I_1, I_2) = \frac{1}{XY}\sum_{x=0}^{X-1}\sum_{y=0}^{Y-1} log(|I_1(x,y) - I_2(x,y)|+1) \tag{3}$$

where X and Y are the horizontal and vertical dimensions of the image in pixels, respectively. While being an uncommon metric, our experiments have shown that this similarity metric significantly outperformed any of the above metrics for our microscopy image sets.

As previously stated, in addition to the non-rigid deformation maximizing the similarity between the registered image and the reference image, the deformation must be realistic and smooth. To constrain the deformation field to be smooth, a penalty term that regularizes the transformation is introduced into the cost function as [5, 6]:

This work was supported by a George M. O'Brien Award from the National Institutes of Health NIH/NIDDK P50 DK 61594.

$$C_{smooth} = \frac{1}{XY}\int_0^X \int_0^Y \left[\left(\frac{\partial^2 \mathbf{T}}{\partial x^2}\right)^2 + \left(\frac{\partial^2 \mathbf{T}}{\partial y^2}\right)^2 + 2\left(\frac{\partial^2 \mathbf{T}}{\partial x \partial y}\right)^2 \right] dx\, dy \quad (4)$$

This regularization is necessary because each pixel in the image is free to move independently. In an extreme case, it is possible that all pixels with one particular intensity in the moving image may map to a single pixel having this same intensity in the reference image, causing the resulting deformation field to be unrealistic [7]. This is one of the primary reasons why non-rigid image registration is considered difficult, as an appropriate balance and compromise must be reached between allowing large amounts of independent movement and ensuring smoothness of the transformation.

Combining these two metrics, the total cost function is given as:

$$C_{total} = C_{sim}\left(I'_{n-1}(x,y), I_n(\mathbf{T}(x,y))\right) + \lambda C_{smooth}(\mathbf{T}) \quad (5)$$

where n denotes the current image number, I' denotes the registered image, and λ is a weighting coefficient which defines the trade-off between the two competing cost terms. To maximize image similarity after registration, and to minimize sharp warping elements in the transformation $\mathbf{T}$, we desire to minimize C_{total}.

This registration method also assumes grayscale, single channel images, not multi-channel images. Therefore, for multi-channel data sets, a particular channel must be selected for registration. Simply using one of the multiple channels directly may be enticing due to its simplicity. However, using only one of the channels and discarding the remaining channels omits much information which may cause improper image registration in these discarded channels. We have obtained results with higher registration accuracy using a composite gray channel, I_{gray}, that is similar to the luminance component of each image. This new gray image is defined as:

$$I_{gray} = \frac{r}{r+g+b} I_{red} + \frac{g}{r+g+b} I_{green} + \frac{b}{r+g+b} I_{blue} \quad (6)$$

where $r = \sum_m \sum_n I_{red}(m,n)$, $g = \sum_m \sum_n I_{green}(m,n)$, and $b = \sum_m \sum_n I_{blue}(m,n)$. Then, for each image, a final deformation field based on the gray image is obtained. This deformation field is then used to transform all channels of the image.

Since intravital microscopy data sets consist of entire stacks of images, non-rigid registration is performed on an image by image basis. In this case, for the current image (or moving image), the reference image is simply not the prior image in the stack. Instead, the reference image used is the registered or warped prior image. This ensures that each image is warped only once so that images do not undergo additional interpolation from multiple warpings.

The degree of deformation allowed is not only affected by the choice of λ, but also by the choice of δ_x, δ_y. The resolution of the grid of control points affects how readily C_{sim} may be minimized. A large, sparse spacing of control points corresponds with a more global non-rigid deformation, which may not allow C_{sim} to reach values near zero. Alternatively, a small, dense spacing of control points corresponds with highly local non-rigid deformations and more readily allows C_{sim} to reach values near zero, but may also encourage more unrealistic deformations. In our work, we have experimented with various grid spacings, and have found that spacings that work well are highly dependent on image size, the content of these images, and the degree of motion artifacts present throughout the stack of images.

Table 1: Single-stage non-rigid registration results

Registration parameters	Percent Improvement using SSD	Percent Improvement using GC
$\delta_x = \delta_y = 128$	55.8%	197.7%
$\delta_x = \delta_y = 64$	61.5%	258.9%
$\delta_x = \delta_y = 32$	64.3%	299.3%
$\delta_x = \delta_y = 16$	64.9%	304.6%

It has been observed that some regions of the images being registered may benefit from a coarse grid spacing, while other regions may benefit from a fine grid spacing. Therefore, rather than using a single grid spacing for our control points, we use a multi-resolution/multi-level approach in a coarse-to-fine strategy. Non-rigid registration is first performed using a control lattice with a coarse grid spacing to account for slowly changing deformations. Next, a control lattice with a finer grid spacing is used to account for more localized and quickly changing deformations. The registered images resulting from a coarse grid spacing are registered again using a fine grid spacing. Additional non-rigid registration iterations using a control lattice with increasingly finer grid spacings may be performed until the user achieves no further improvement in image registration. We will show that this multi-resolution approach is able to achieve more accurate matching between a registered image and its reference image.

3. EXPERIMENTAL RESULTS

We demonstrate our multi-resolution non-rigid registration method on a stack of approximately 150 images collected in time-series from the lung of a living rat.[1] Motion artifacts present an enormous challenge for intravital microscopy. In order to reconstruct a three-dimensional volume from a series of images collected over a range of depths in a tissue, or to quantify dynamic changes in fluorescence in a series of images collected from the same structure over time, motion-induced artifacts resulting from respiratory and cardiac function must be eliminated. Figure 1(a) shows a single image from this stack.

We first use non-rigid registration using a single-stage process, where only one control point spacing is used. We use this method for multiple trials with a variety of spacings, including 128, 64, 32, and 16 pixels between control points. After registration, we determine the average of both sum of squared differences (SSD) of pixel intensities and sum of gradient correlation (GC) across all images in the sequence as quantitative measures of registration performance [9]. We choose metrics that are unrelated to the similarity metric used in the cost function. Results for this image sequence are shown in Table 1 which compares the SSD and GC before and after single-stage registration. For all of these trials, we empirically choose $\lambda = 0.01$, as it demonstrated the best results over a wide range of possible values. We see that non-rigid registration has significantly improved image alignment. Note that using a densely spaced grid of control points, which permits increased bending and warping to correct more intense motion artifacts, slightly improves image alignment. However, this is not necessarily true for all data sets. With the transformation able to deform more rapidly, particular control points during the optimization may be more likely to become attracted to local minimums rather than global minimums.

[1] Data provided by Dr. Irina Petrache, Indiana University School of Medicine, as part of the collaboration that resulted in [8].

Table 2: Two-stage non-rigid registration results

Registration parameters	Percent Improvement using SSD	Percent Improvement using GC
$\delta_x^{(1)} = \delta_y^{(1)} = 128$ $\delta_x^{(2)} = \delta_y^{(2)} = 64$	67.6%	293.1%
$\delta_x^{(1)} = \delta_y^{(1)} = 64$ $\delta_x^{(2)} = \delta_y^{(2)} = 32$	71.5%	341.4%
$\delta_x^{(1)} = \delta_y^{(1)} = 32$ $\delta_x^{(2)} = \delta_y^{(2)} = 16$	73.7%	364.1%
$\delta_x^{(1)} = \delta_y^{(1)} = 16$ $\delta_x^{(2)} = \delta_y^{(2)} = 8$	74.0%	365.8%

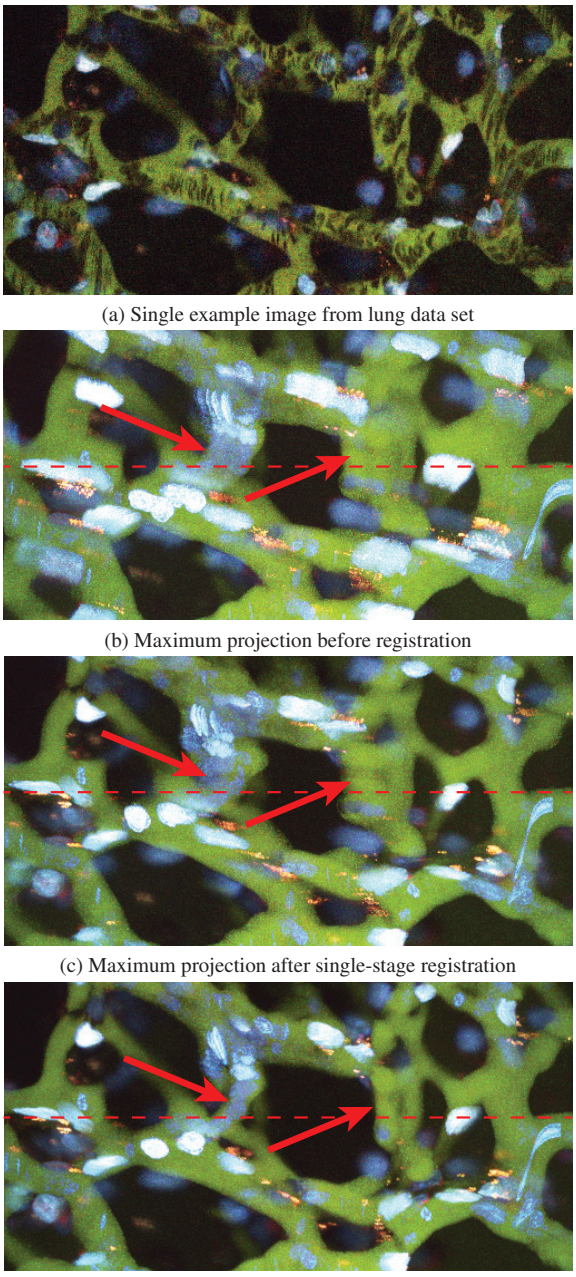
Table 3: Three-stage non-rigid registration results

Registration parameters	Percent Improvement using SSD	Percent Improvement using GC
$\delta_x^{(1)} = \delta_y^{(1)} = 128$ $\delta_x^{(2)} = \delta_y^{(2)} = 64$ $\delta_x^{(3)} = \delta_y^{(3)} = 32$	74.2%	368.8%
$\delta_x^{(1)} = \delta_y^{(1)} = 64$ $\delta_x^{(2)} = \delta_y^{(2)} = 32$ $\delta_x^{(3)} = \delta_y^{(3)} = 16$	76.4%	393.4%
$\delta_x^{(1)} = \delta_y^{(1)} = 32$ $\delta_x^{(2)} = \delta_y^{(2)} = 16$ $\delta_x^{(3)} = \delta_y^{(3)} = 8$	77.8%	407.2%

Next, we use the proposed multi-resolution approach and execute non-rigid registration in multiple stages, using multiple grid spacings in a coarse-to-fine manner. For an arbitrary number of stages in the multi-resolution process, the grid spacings for the horizontal and vertical directions for the n-th stage are denoted $\delta_x^{(n)}$ and $\delta_y^{(n)}$, respectively. We begin with a two-stage registration, with $\delta_x^{(2)} = \delta_x^{(1)}/2$ and $\delta_y^{(2)} = \delta_y^{(1)}/2$. Again, we choose a variety of spacings, including 128, 64, 32, and 16 pixels between control points for $\delta_x^{(1)}, \delta_y^{(1)}$. Results comparing the SSD and GC for this two-stage process are shown in Table 2. We notice that the percent improvements in average SSD and GC per image have increased substantially when comparing similar grid spacings for single-stage registration. A multi-resolution approach has improved image alignment with minimal computational cost.

To further improve image alignment, we investigate three-stage registration, with $\delta_x^{(3)} = \delta_x^{(2)}/2 = \delta_x^{(1)}/4 =$ and $\delta_y^{(3)} = \delta_y^{(2)}/2 = \delta_y^{(1)}/4$. As before, we choose a variety of spacings, including 128, 64, and 32 pixels between control points for $\delta_x^{(1)}, \delta_y^{(1)}$. Results comparing the SSD and GC for this three-stage process are shown in Table 3. Note that the percent improvements in average SSD and GC per image have increased, but not as much compared with the two-stage registration process. One drawback of using an additional stage in the registration is that the registered images undergo an additional interpolation stage, possibly blurring and obscuring important cellular structures. One may argue that the percent improvements in SSD and GC are not beneficial enough to offset the loss in image sharpness. Two-stage registration appears to be a moderate compromise between registration accuracy and image quality.

To obtain a more qualitative and visual evaluation of registration accuracy, we compare maximum projection images from before registration, after single-stage registration, and after two-stage registration. Maximum projection images are assembled by pixel-wise comparison of the intensities of each of the images in the stack and retaining the largest value. For ideally registered images, structures will have perfectly sharp edges with no ghosting or smearing in the maximum projection images. In contrast, before registration, we see in Figure 1(b) that the maximum projection image exhibits distinct blurring of object edges, indicating severe misalignment of objects. Particular areas of interest that exhibit large amounts of smearing are indicated by the two arrows. Figure 1(c) shows that single-stage registration has improved the alignment of cellular structures as the smeared appearance has been reduced. Comparing the same areas of interest indicated by the two arrows, we see that the vasculature is narrower and has more sharply defined edges, indicating improved



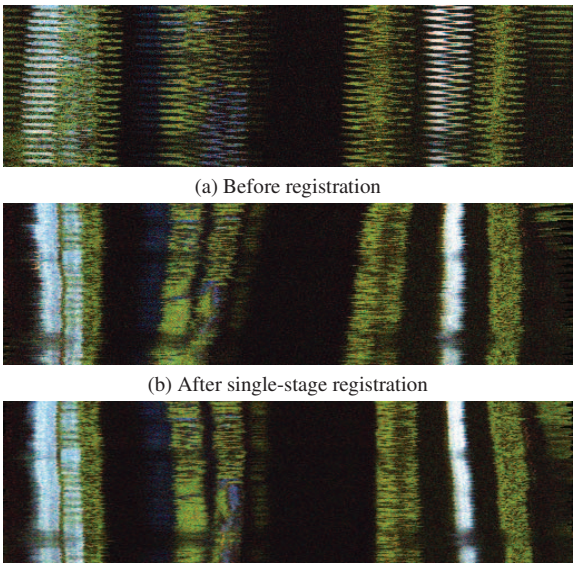
(a) Single example image from lung data set

(b) Maximum projection before registration

(c) Maximum projection after single-stage registration

(d) Maximum projection after two-stage registration

Fig. 1: Maximum projection images of registration results. Image field is 205 μm wide.



(a) Before registration

(b) After single-stage registration

(c) After two-stage registration

Fig. 2: Line projection images of registration results. Image field is 205 μm wide.

image alignment. However, in Figure 1(d), after two-stage registration, the maximum projection image shows incredible and vast improvement of object alignment compared to Figure 1(b), indicating extraordinary reduction of the motion artifacts in the original image series. The two areas of interest confirm this by showing further improvement in image alignment with significantly increased edge sharpness and increased narrowness of the vasculature.

As an additional visual comparison, line scan projection images are created from before registration, after single-stage registration, and after two-stage registration. Line scan projection images are assembled by selecting a single line of pixels as one axis and plotting this against time/depth on the other axis. These images are shown in Figure 2, with the line selected to create the projection image shown as a dashed line in Figure 1. For ideally registered images, we should see perfect aligned, solid, continuous, vertical structures in the line projection images. In contrast, before registration, we see in Figure 2(a) that the line scan projection exhibits disjointed cellular structures as there is distinct back-and-forth motion. In Figure 2(b), after single-stage registration, the two nuclei labeled in blue on both the left and right side of the image show much improved vertical continuity. However, the vasculature labeled in green in the middle of the projection image exhibit drifting. In Figure 2(c), after two-stage registration, both the nuclei and vasculature show continuity and no drifting and are vastly improved compared to Figure 2(a) and Figure 2(b). We have used both the SSD metric for quantitative evaluation, and maximum projection and line scan projection images for qualitative evaluation in our previous work [10].

4. CONCLUSION

We have described a non-rigid image registration method using B-splines to improve the quality of images collected in intravital microscopy, supporting both reconstruction of three-dimensional images and quantitative analyses of images collected in time-series. This is achieved by using multi-resolution non-rigid registration to reduce motion artifacts and improve image alignment, according to both quantitative SSD and GC metrics and visual evaluation. A two-stage registration process provides significant improvement to registration accuracy over a single-stage process. A three-stage registration process allows further improvement in registration accuracy, but may degrade image quality. The computational runtime of our method is approximately 1-3 minutes per image in the series per stage, depending on image size and δ_x, δ_y. We are examining automated approaches to determine the appropriate number of stages in a multi-resolution approach, along with the optimal grid density.

5. REFERENCES

[1] D. Rueckert, L. I. Sonoda, C. Hayes, D. L. G. Hill, M. O. Leach, and D. J. Hawkes, "Nonrigid registration using free-form deformations: Application to breast MR images," *IEEE Transactions on Medical Imaging*, vol. 18, no. 8, pp. 712–721, August 1999.

[2] Y. Mazaheri, L. Bokacheva, D.-J. Kroon, O. Akin, H. Hricak, D. Chamudot, S. Fine, and J. A. Koutcher, "Semi-automatic deformable registration of prostate MR images to pathological slices," *Journal of Magnetic Resonance Imaging*, vol. 32, no. 5, pp. 1149–1157, April 2010.

[3] S. Lee, G. Wolberg, and S. Shin, "Scattered data interpolation with multilevel b-splines," *IEEE Transactions on Visualization and Computer Graphics*, vol. 3, no. 3, pp. 228–244, July-September 1997.

[4] M. Unser, "Splines: A perfect fit for signal and image processing," *IEEE Signal Processing Magazine*, vol. 16, no. 6, pp. 22–38, November 1999.

[5] C. O. S. Sorzano, P. Thévenaz, and M. Unser, "Elastic registration of biological images using vector-spline regularization," *IEEE Transactions on Biomedical Engineering*, vol. 52, no. 4, pp. 652–663, April 2005.

[6] T. Rohlfing, C. R. Maurer Jr., D. A. Bluemke, and M. A. Jacobs, "Volume-preserving nonrigid registration of MR breast images using free-form deformation with an incompressibility constraint," *IEEE Transactions on Medical Imaging*, vol. 22, no. 6, pp. 730–741, June 2003.

[7] X. Pennec, P. Cachier, and N. Ayache, "Understanding the "Demon's Algorithm": 3D Non-rigid registration by gradient descent," *Proceedings of the Second International Conference on Medical Image Computing and Computer-Assisted Intervention, Cambridge, UK*, pp. 597–605, 1999.

[8] R. G. Presson Jr, M. B. Brown, A. J. Fisher, R. M. Sandoval, K. W. Dunn, K. S. Lorenz, E. J. Delp, P. Salama, B. A. Molitoris, and I. Petrache, "Two-photon imaging within the murine thorax without respiratory and cardiac motion artifact," *The American Journal of Pathology*, vol. 179, no. 1, pp. 75–82, 2011.

[9] G. P. Penney, J. Weese, J. A. Little, P. Desmedt, D. L. G. Hill, and D. J. Hawkes, "A comparison of similarity measures for use in 2-D-3-D medical image registration," *IEEE Transactions on Medical Imaging*, vol. 17, no. 4, pp. 586–595, August 1998.

[10] K. S. Lorenz, P. Salama, K. W. Dunn, and E. J. Delp, "Digital correction of motion artefacts in microscopy image sequences collected from living animals using rigid and nonrigid registration," *Journal of Microscopy*, vol. 245, no. 2, pp. 148–160, February 2012.